



Detecting moisture transport pathways to the subtropical North Atlantic free troposphere using paired H_2O - δD in situ measurements

Yenny González^{1,2,a}, Matthias Schneider³, Christoph Dyroff^{3,b}, Sergio Rodríguez², Emanuel Christner³, Omaira Elena García², Emilio Cuevas², Juan Jose Bustos², Ramon Ramos², Carmen Guirado-Fuentes², Sabine Barthlott³, Andreas Wiegeler³, and Eliezer Sepúlveda²

¹Sieltec Canarias, S. L., Hábitat 2, 38204, San Cristóbal de La Laguna, Santa Cruz de Tenerife, Canary Islands, Spain

²Izaña Atmospheric Research Centre (IARC), Agencia Estatal de Meteorología (AEMET), Santa Cruz de Tenerife, Canary Islands, Spain

³Institute of Meteorology and Climate Research (IMK-ASF), Karlsruhe Institute of Technology (KIT), Karlsruhe, Germany

^anow at: Dept. of Earth, Atmospheric and Planetary Sciences, Massachusetts Institute of Technology, 77 Massachusetts Avenue, Cambridge, MA 02139-4307, USA

^bnow at: Aerodyne Research Inc., 45 Manning Road, Billerica MA 01821, USA

Correspondence to: Yenny González (yglezram@mit.edu)

Received: 13 August 2015 – Published in Atmos. Chem. Phys. Discuss.: 8 October 2015

Revised: 15 March 2016 – Accepted: 17 March 2016 – Published: 5 April 2016

Abstract. We present two years of in situ measurements of water vapour (H_2O) and its isotopologue ratio (δD , the standardized ratio between H_2^{16}O and HD^{16}O), made at two remote mountain sites on Tenerife in the subtropical North Atlantic. We show that the data – if measured during night-time – are well representative for the lower/middle free troposphere. We use the measured H_2O - δD pairs, together with dust measurements and back trajectory modelling for analysing the moisture pathways to this region. We can identify four principally different transport pathways. The air mass transport from high altitudes and high latitudes shows two different scenarios. The first scenario brings dry air masses to the stations, as the result of condensation events occurring at low temperatures. The second scenario brings humid air masses to the stations, due to cross-isentropic mixing with lower-level and more humid air during transport since last condensation (LC). The third pathway is transportation from lower latitudes and lower altitudes, whereby we can identify rain re-evaporation as an occasional source of moisture. The fourth pathway is linked to the African continent, where during summer, dry convection processes over the Sahara very effectively inject humidity from the boundary layer to higher altitudes. This so-called Saharan Air Layer (SAL) is then advected westward over the Atlantic and contributes to moisten the free troposphere. We demon-

strate that the different pathways leave distinct fingerprints on the measured H_2O - δD pairs.

1 Introduction

In the subtropical free troposphere, in the region of the descending branch of the Hadley cell, the humidity is not conserved along the mean subsidence (Pierrehumbert, 1998). Instead, this dry air is often moistened (Galewsky and Hurley, 2010; Couhert et al., 2010; Risi et al., 2012). The few studies based on atmospheric modelling points to the turbulent transport of water vapour from the surface upwards as the dominant moistening process, balancing the drying in the subtropical free troposphere (Couhert et al., 2010; Risi et al., 2012). Additional processes, such as evaporation of condensate and isentropic eddy transport of moist air from the tropics, are suggested to also contribute to moisture in this region (Galewsky and Hurley, 2010, and references therein), but the sources and dynamics involved in this moistening are still unclear.

Several studies indicate that water vapour isotopologue observations are very promising for investigating the different moisture pathways in this region. Such observations can be used to distinguish between the different mechanisms as-

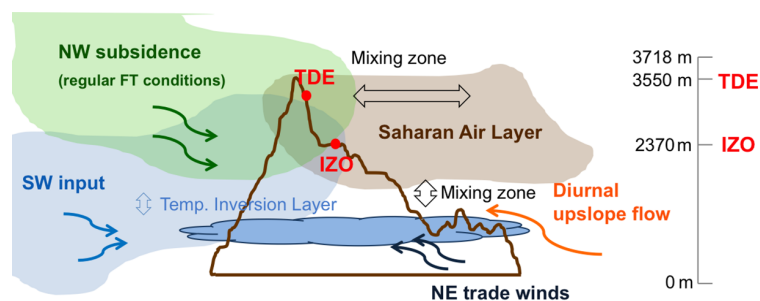


Figure 1. Schematic depiction of the processes influencing the water vapour balance over Tenerife in the subtropical North Atlantic. A temperature inversion layer separates the marine boundary layer (MBL) and the free troposphere (FT). In the MBL, NE trade winds blow, while in the FT, the regular NW subsidence regime is alternated in summer with Saharan dust outbreaks. On the island, the upslope winds prompt MBL air to reach the low FT during the daytime. IZO and TDE stations are represented as red dots.

sociated with moistening (e.g. Galewsky and Hurley, 2010; Noone et al., 2011; Tremoy et al., 2012; Samuels-Crow et al., 2014; Bailey et al., 2013, 2015; Dyroff et al., 2015; Steen-Larsen et al., 2015; Schneider et al., 2015). Stations located in the subtropical free troposphere are key emplacements for studying the synoptical scale humid transport in the subtropics. Studies based on water vapour isotope observations in the subtropical Pacific free troposphere highlight the relevance of moisture exchange between the boundary layer and the free troposphere due to shallow convection at local scale (Bailey et al., 2013). In addition, subtropical moisture is strongly affected by the mixing of air masses, with humidity properties that are defined by their condensation and evaporation history on a regional scale (Noone et al., 2011). In the North Atlantic, studies based on in situ water vapour isotopologue measurements have been focused on the moisture sources influencing the marine boundary layer (Benetti et al., 2014; Steen-Larsen et al., 2014, 2015). However, studies in relation to transport pathways of moisture in the subtropical North Atlantic free troposphere including long-term measurements of water vapour isotopologues have not been reported yet. In contrast to the Pacific, the atmosphere over the subtropical North Atlantic is regularly affected by dust outbreaks (from the Sahara desert) and consequently, the scheme of moisture exchange in the subtropical Pacific region can not fully describe those occurring in the subtropical North Atlantic. In order to fill this gap, we present and discuss the first multi-year observational in situ data set of free-tropospheric water vapour isotopologues in the subtropical North Atlantic region.

In the following we express the isotopologues H₂¹⁶O and HD¹⁶O as H₂O and HDO. The δ-notation expresses the per mil difference of the stable isotope ratio of a water sample ($R = \text{HDO}/\text{H}_2\text{O}$) from that of the isotope ratio of Vienna Standard Mean Ocean Water, i.e. $\delta\text{D} = 1000 \times (R/R_{\text{VSMOW}} - 1)$ ($R_{\text{VSMOW}} = 3.1152 \times 10^{-4}$, Craig, 1961; Coplen, 2011).

In Sect. 2 of this paper we present the measurement sites and discuss the methodology of our study. In Sect. 3 we doc-

ument that our night-time measurements are representative for the subtropical North Atlantic lower free troposphere. We use backward trajectories and dust measurements as tracers for detecting the main meteorological processes. Then, we document that these processes leave unique fingerprints in the H₂O-δD distribution. Section 4 summarizes the work.

2 Methodology

2.1 Measurement site

As a study area we used Tenerife (Canary Islands, Spain; 28.3° N, 16.5° W). On this island, two high mountain sites are run by the Izaña Atmospheric Research Centre. IZO (Izana Observatory) is a mountain top station located at 2367 m a.s.l., whereas TDE (Teide Observatory) is a small measurement site located at the volcanic cone at 3550 m a.s.l. In the context of the project MUSICA (MULTi-platform remote Sensing of Isotopologues for investigating the Cycle of Atmospheric water), we installed two Picarro instruments at IZO and TDE stations. These instruments provide continuous isotopologues data for altitudes above 2000 m, which are unique for the subtropical North Atlantic.

A schematic depiction of the locations of IZO and TDE and the meteorological processes affecting the measurement sites are shown in Fig. 1. In the subtropical North Atlantic region, the atmospheric stability is determined by the combination of two synoptic processes that well define the marine boundary layer (MBL) and the free troposphere (FT). In the MBL, a quasi-permanent north-north-east (NNE) trade wind blows (< 1000 m a.s.l., Palmén and Newton, 1969). In the FT, the descendent branch of the Hadley cell around 30° N results in a north-western (NW) subsidence regime (Galewsky et al., 2005; Cuevas et al., 2013). This subsidence is frequently alternated in summer with south-eastern (SE) Saharan dust outbreaks (Chiapello et al., 1999). Episodes of air mass transport from a south-westerly (SW) direction are also occasionally observed.

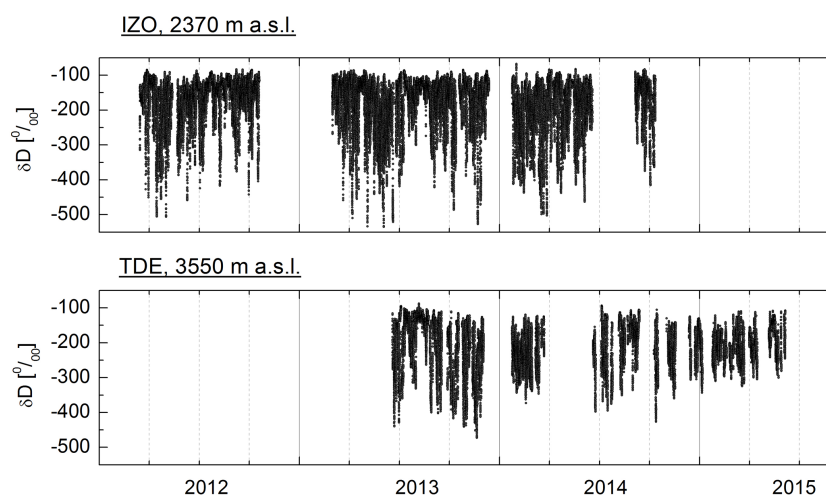


Figure 2. Time periods covered by water isotopologue in situ observations at IZO (upper panel) and TDE (lower panel). All 10 min averages of δ D measured at any time of the day are shown.

The local moisture exchange between the MBL and the FT is limited by a temperature inversion layer. In the surroundings of the island, the top of the MBL, which is frequently located just below the temperature inversion layer, is characterized by a stratocumulus layer formed by the condensation of water vapour onto the pre-existing particles (Rodríguez et al., 2009). This layer creates a quasi-continuous foggy and rainy regime between 800 and 2000 m a.s.l., which is more pronounced on the northern part of the island. The effectiveness of this layer in separating the MBL from the FT is reflected in the relative humidity (RH) profile. In the FT, the RH is typically around 20 %, whereas it is normally above 60 % in the MBL (Cuevas et al., 2013). Vertical mixing between MBL and FT air is observed during the daytime due to the upslope flow regime (taking place on a very local scale).

2.2 Measurements of water vapour isotopologues

Two commercial cavity ring-down spectrometers (Picarro model L2120-I) have been used for water vapour isotopologues, monitoring at the two mountain sites on Tenerife. At IZO, measurements started in March 2012 and at TDE in July 2013. The data sets consist of about 75 000 (at IZO) and 40 000 (at TDE) 10 min averages. Time series of δ D measurements at IZO and TDE stations are shown in Fig. 2. The measurement gaps are due to instrument failure, maintenance, and shut downs due to extreme weather conditions. Although during summer data have been registered almost continuously, the measurements have often been interrupted during winter. There are only a few measurement days in December and January (at IZO) and in January (at TDE).

At IZO, H₂O data between 200 and 16 000 ppmv and δ D between -500 and -90 ‰ were recorded. At TDE, H₂O ranged between 250 and 12 000 ppmv and δ D ranged between -430 and -100 ‰. At Mauna Loa free troposphere sta-

tion, Noone et al. (2011) reported δ D values between -100 and -400 ‰ and humidities between 500 and 15 000 ppmv. On the Chilean hyperarid Chajnantor plateau, Samuels-Crow et al. (2014) recorded H₂O- δ D pairs ranging from 95 ppmv and -465 ‰ to 12 500 ppmv and -45 ‰. Thus, the in situ H₂O- δ D measurements made at the different subtropical free-tropospheric stations registered data that are within the same order of magnitude.

At IZO, the sampling inlet is installed 4 m above the roof of a 6-floor building at a height of 30 m above ground (2397 m a.s.l.). It consists of a stainless steel tube of 18 m that goes from the terrace of the tower, through the service channel to the Picarro laboratory. A vacuum pump generates an inflow of 2810 L min⁻¹ (standard conditions) throughout the sampling line, which has an inner diameter of 80 mm. The manifold has an inner diameter of 80 mm and a length of 250 mm. The instrument takes the air sample using a stainless steel tube with an inner diameter of 4 mm, which goes from the manifold to the inlet of the analyzer (1.6 m). An additional pump with an inflow of 5 L min⁻¹ is connected in series at the inlet of the instrument. The residence time of the air inside the tubing is approximately 8 s.

At TDE, the inlet is also 4 m above the roof at a height of 6 m above the ground (3556 m a.s.l.). The sampling line is connected to a manifold with an inner diameter of 60 mm and a total length of 5 m where the air is pumped at 20 L min⁻¹. The air then flows to the instrument through stainless steel tubes with an inner diameter of 4 mm (3.3 m). At TDE, an additional pump with an inflow of 5 L min⁻¹ is also connected in series at the inlet of the instrument. The residence time of the air is approximately 44 s.

No heated tubing was implemented at any of the stations. The relative humidity values were above 90 % for only 7.6 % and 4.6 % of the data at IZO and TDE stations. In these conditions, the outside temperature at IZO ranges between -6

and 15°C, whereas at TDE it varies between 6 and 11°C. Since the tubing in the buildings is kept around 21°C, condensation events in the inlet lines can be excluded.

For calibration purposes we used two liquid working standards of composition $\delta D_{S1} = -142.2 \pm 0.7$ ‰ and $\delta D_{S2} = -245.3 \pm 0.7$ ‰. The working standards were prepared from a mixture of ground water from Karlsruhe, Germany, melted Antarctic snow (S1), and the pure melted Antarctic snow (S2). The isotopologue composition of these standards was measured by Le Laboratoire des Sciences du Climat et de l'Environnement (LSCE-CEA, France) and referenced to the VSMOW2/SLAP2 scale (IAEA, 2009). For routine measurements we need a significant amount of liquid standards (1 L year⁻¹ and instrument). Large amounts of our two standards are available and we can perform continuous calibrations during long measurement periods.

The instruments are calibrated every 8–12 h using liquid standards injected with the Picarro Standards Delivery Module (SDM). The instrument precision for 10 min averages and at 15 700 ppmv is better than 0.2‰ (see Aemisegger et al., 2012, Fig. 7a), and for very dry conditions within a few permil. The error estimation accounts for the described instrument precision as well as errors due to the following corrections:

- uncertainty of the standards (0.7‰ for both),
- humidity dependence (from 0.3‰ for 10 000 ppmv, up to 8.0‰ at 200 ppmv),
- extrapolation of VSMOW2-SLAP2 scale outside the range of calibration (for humid air: < 2.0‰; up to 5‰ for strong depleted, i.e. generally dry air),
- calibration (1‰ for the whole humidity range).

The absolute uncertainties in δ D are then < 15‰ at 500 ppmv, < 4‰ at 4500 ppmv and even smaller for higher humidity. More detailed information about the calibration procedure, stability, and uncertainty estimations of the two instruments is given in Appendix A.

The leading errors are due to the calibration corrections, meaning that they are systematic errors for the period between two calibrations. Thus, calculating 1 or 3 h averages instead of 10 min averages will not significantly reduce these errors. Actually, the variations we see within 1 h are mostly real atmospheric variations (recall the high precision of the 10 min averages). Calculating averages of these real atmospheric small-scale variations is not trivial and might affect the H₂O- δ D distribution: firstly, H₂O is often log-normally distributed and it will make a difference whether we use the mean or the median H₂O concentrations. Secondly, H₂O- δ D pairs do not vary along a single straight line. By averaging the δ D and the H₂O values, the averaged H₂O- δ D data point will be below the mixing line or the Rayleigh curve described by the individual data points. If we average the δ D weighted by H₂O, the pairs will lie close to the mixing line, but we will

not capture the situation of a Rayleigh process well. In order to avoid artefacts caused by data averaging, all the H₂O- δ D distribution plots of our study are made with high resolution data (10 min averages).

2.3 Measurements of dust

Long-term measurements of aerosol at Izaña include chemical composition, dust concentrations, and size distribution. The methodology and quality control of aerosol in situ techniques are described in Rodríguez et al. (2012). In Izaña, bulk mass concentrations of aerosols are clearly dominated by Saharan dust (Basart et al., 2009; Rodríguez et al., 2011). We used records of dust at Izaña to detect the arrival of north African air (Rodríguez et al., 2012).

Unfortunately, in situ dust measurements are not available at TDE. In order to distinguish between clean and dust-laden conditions at this station we use the AERONET columnar-integrated aerosol optical depth (AOD) level 2.0 obtained at a wavelength of 500 nm at IZO (<http://aeronet.gsfc.nasa.gov>). See more details of calibration procedures, data acquisition, and processing in Holben et al. (1998).

2.4 Back trajectories

Transport pathways of moisture are analysed by integrating the Global Data Assimilation System archive information (GDAS1, NCEP) in the Hybrid Single Particle Lagrangian Integrated Trajectory model (HYSPLIT 4.0). The GDAS1 is available every 6 h, and the post-processing converts the data to 1° × 1° latitude–longitude grids and from sigma levels to the 23 pressure levels between 1000 and 20 hPa (Rolph et al., 2014). HYSPLIT performs a linear interpolation between the times of the available input data (6 h) for calculating 5-day back trajectories of 1 h resolution (Draxler and Rolph, 2003). The trajectories are released at the height above sea level of the stations. The vertical component of the back trajectories was computed using the vertical model velocity. The end points of the trajectories were set at Tenerife (28.3° N, 16.5° W) at the elevations of the IZO and TDE stations.

3 Results

3.1 The effect of the local diurnal upslope flow

The airflow regime at IZO is driven by the occurrence of upward transport of humid air during the daytime and downward transport of dry FT air at night. The upward transport is caused by the combination of the thermally driven growth of the MBL volume and the buoyant airflows caused by the heating of the air located just above the terrain (Rodríguez et al., 2009). This upslope flow transports the gases emitted on lower parts of the island, which is captured in the marked daily cycle of gases and particles measured at IZO

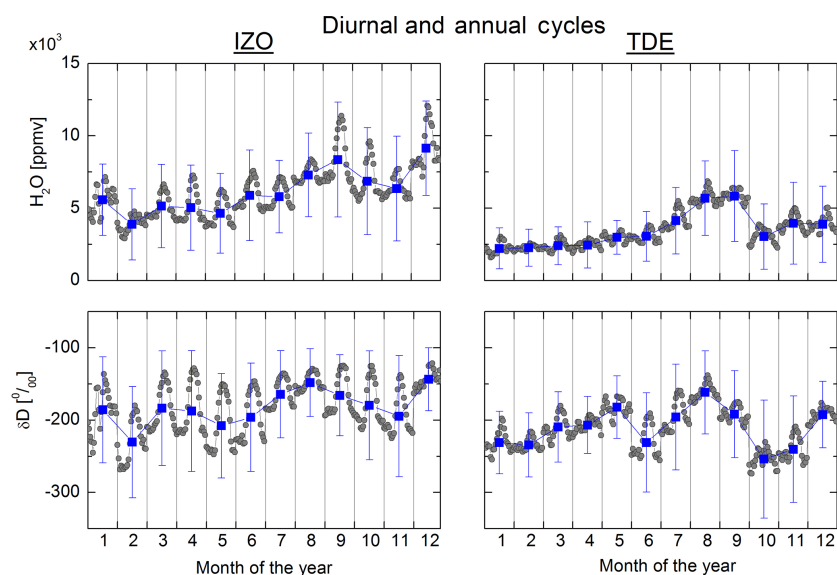


Figure 3. The mean diurnal cycle and annual cycles of H₂O-δD (left panels for IZO and right panels for TDE). Grey dots show the mean diurnal cycles for each month (mean value for each hour of the day) and the blue squares the annual cycle (mean and standard deviation of all observations that fall within an individual month).

(e.g. Rodríguez et al., 2009). The highest concentrations of pollutants are observed in the early afternoon.

Figure 3 shows the monthly mean daily cycle of H₂O and δD at IZO and TDE stations respectively (grey dots). The annual mean and standard deviation of H₂O and δD at both stations is also shown in blue dots. There is a marked daily cycle in the H₂O and δD data of the IZO station (left column in Fig. 3) and a weaker one at the TDE station (right column in Fig. 3). At IZO, the diurnal cycle of H₂O and δD is more pronounced than the annual cycle. At TDE, the H₂O annual cycle is stronger than the diurnal cycle. However at TDE, δD data also show a diurnal cycle with an amplitude similar to the amplitude of the annual cycle.

The distribution of the 10 min H₂O-δD pairs collected at IZO and TDE stations are shown in Fig. 4. The whole data set (10 min average) is presented in grey dots; black dots represent the data collected during night-time (from midnight to 1 h after sunrise). Orange crosses represent the data collected during the daytime (from 3 to 10 h after sunrise, when the upslope breeze is active).

At IZO, the lowest δD values are measured at night-time (Fig. 4). During the daytime, we observe less depletion. The H₂O-δD pairs measured at IZO during the daytime are assembled in the upper side of the H₂O-δD distribution ($\delta D = -146 \pm 39 \text{ ‰}$, orange crosses, left column in Fig. 4). At mid-day, the increase of humidity is associated with a mean isotopic composition of $\delta D = -131 \pm 35 \text{ ‰}$. This value is similar to the one measured close to the ocean by Dyroff et al. (2015). The δD mean value of these in-flight measurements measured around the top of the MBL, 600–900 m a.s.l. in front of the Tenerife coast was $-124 \pm 43 \text{ ‰}$. Thus, the shift-

ing of the H₂O-δD pairs to the upper side of the distribution is the result of the mixing of dry FT air with water evaporated from the surrounding ocean and exported by turbulent mixing to the top of the MBL. This result is in agreement with the one found by Noone et al. (2011) in Mauna Loa (Hawaii).

At TDE, the difference between the daytime and night-time H₂O-δD distribution is not as clear as at IZO (right column in Fig. 4). The weaker diurnal effect at TDE station is due to its location. TDE is located at a higher altitude on a rather sharp peak (Pico del Teide). There it is less exposed to the slope breezes and consequently, the influence of the MBL-FT air mixing is weaker.

At IZO, gases and particles measured at night-time well represent FT conditions (Gómez-Peláez et al., 2006; Rodríguez et al., 2009, 2012; Cuevas et al., 2013). To examine the variability of the H₂O-δD pairs in the subtropical North Atlantic FT, and in order to avoid the possible local MBL-FT mixing, only the H₂O-δD pairs measured at night-time at IZO and TDE will be considered in the following study.

Appendix B complements this study of the diurnal signals in the H₂O-δD distribution. Figure B1 shows a two-dimensional plot of the density of the H₂O-δD pairs for night-time and daytime observations.

3.2 The Saharan Air Layer and the moisture in the subtropical North Atlantic FT

The meteorological pattern of the subtropical North Atlantic region is characterized by a constant transport of Atlantic air masses that alternate with Saharan dust events, especially in summer. Previous work carried out in this region show that these two regimes can easily be distinguished by

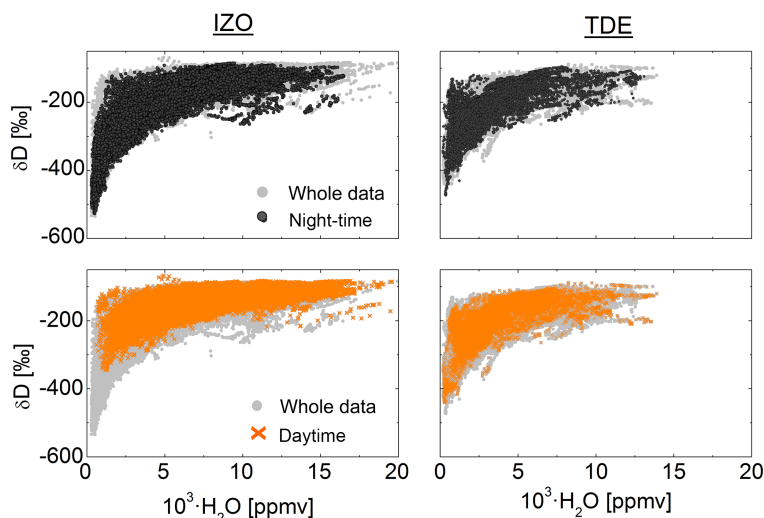


Figure 4. Distribution of the H₂O-δD pairs (10 min averages) at IZO (left) and TDE (right) stations. Grey dots show all data for the individual stations. Black dots represent the data collected during night-time (from midnight to 1 h after sunrise). Orange crosses represent the data collected during the daytime (from 3 to 10 h after the sunrise). The whole data set is presented in grey dots.

their dust content. At IZO, dust concentrations under background clean conditions are lower than $2 \mu\text{g m}^{-3}$ (Rodríguez et al., 2009), whereas during Saharan events, dust concentrations above $25 \mu\text{g m}^{-3}$ are usually observed (Rodríguez et al., 2015). The Izaña AOD levels for background conditions are usually lower than 0.05 (García et al., 2012) and frequently above 0.10 during dust events (Basart et al., 2009; García et al., 2012).

The left column in Figs. 5 and 6 show the distribution of 5 day back trajectories for non-dust and dust-laden conditions at IZO and TDE stations respectively. We considered that an air mass experiences condensation when RH along the trajectory to the station exceeds the limit of 80 % during a 3 h time interval (James et al., 2004; Sodemann et al., 2008). If this occurs, we set this point as the initial point of the back trajectory. If no condensation was observed along the 5-day path, the back trajectory was fully drawn. Clean dust-free air masses originate from the FT over the Atlantic (first row in Figs. 5 and 6). Dust-laden air masses originate in north Africa close to the surface (dust $> 25 \mu\text{g m}^{-3}$, AOD > 0.1 , second row in Figs. 5 and 6).

The right column in Figs. 5 and 6 show the 10 min average H₂O-δD pairs measured under non-dust (green dots) and dust-laden conditions (red dots) at IZO and TDE stations respectively. The whole H₂O-δD distribution (grey dots) is quite well confined within two theoretical curves. The theoretical line on the low δD value side of the distribution represents the evolution of an air mass that has experienced Rayleigh distillation, a gradual dehydration in which all condensate is immediately removed from the vapour phase (initial conditions: RH = 80 % and SST = 25 °C, orange line). The Rayleigh process starts when saturation is reached (dew point). The equations and coefficients for

saturation over water conditions were taken from Johnson et al. (2001). For the theoretical mixing we assume moistening by evaporation from the ocean surface and drying by middle/upper tropospheric air (initial conditions of air mass 1: H₂O = 18 000 ppmv, δD = -84 ‰; air mass 2: H₂O = 400 ppmv, δD = -600 ‰, solid black line). The calculation of this mixing line is based on the simplified solution of the diffusion mixing model shown by Noone et al. (2011, Eq. 6). These two theoretical lines (Rayleigh and mixing) mostly cover the set of H₂O-δD measured during this study.

The H₂O-δD pairs associated with clearly non-dust conditions represent 55 % of the data collected at IZO and 51 % of the data collected at the TDE. The origin of the North Atlantic air masses reaching IZO and TDE stations covers a wide area (0–60° N, 45° W–20° E), and also a wide range of altitudes (0–10 km; left column in Figs. 5 and 6). A wide H₂O-δD distribution is measured under the arrival of dust-free air masses (green dots in right column in Figs. 5 and 6). This distribution illustrates the effect of non-Rayleigh processes affecting H₂O and δD, such as air mass mixing and different H₂O-δD-relations (Rayleigh-curves) of air masses from different source regions (Brown et al., 2013). At both stations, night-time H₂O-δD pairs below a minimum Rayleigh curve for air masses with subtropical origin (initial H₂O = 27 000 ppmv, δD = -71 ‰) cannot be explained by condensation or mixing. Therefore, these occasional super-Rayleigh observations indicate additional fractionation related to either intracloud or subcloud processes or post-condensational exchange (Brown et al., 2013, and references therein). These observations will be discussed later.

Saharan dust conditions (dust $> 25 \mu\text{g m}^{-3}$) were observed in 20 % of IZO and 19 % of TDE of the whole recorded data. At IZO summer data represent 74 % of the Saharan

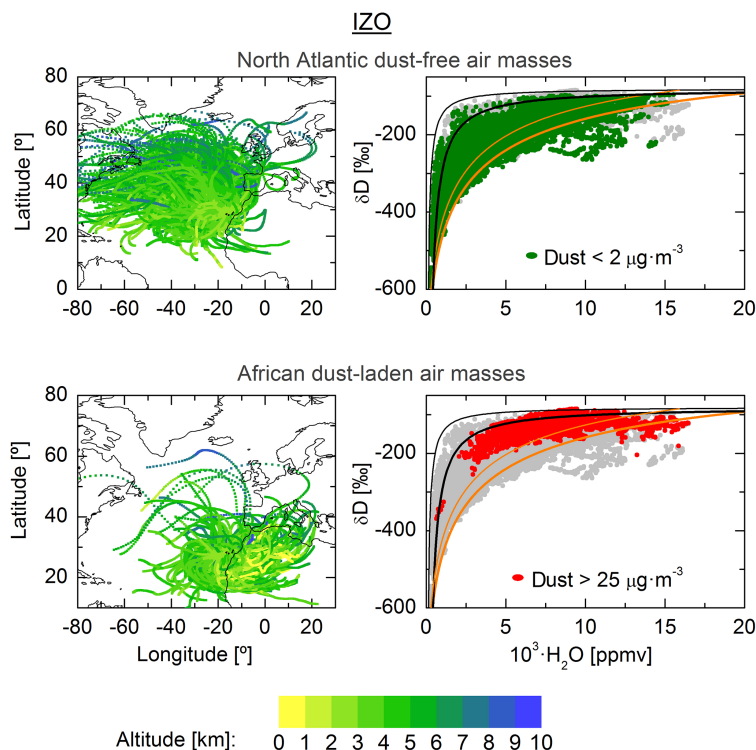


Figure 5. Air masses reaching IZO station as a function of the dust load. First row shows non-dust conditions, second row, dust-laden conditions. The colour-bar indicates the altitude (km) of these air masses in each grid. The left column shows the trajectories. The right column shows the H₂O- δ D distribution (pairs are presented on 10 min average): all data (grey dots), data measured under non-dust conditions (green dots) and data for dust-laden conditions (red dots). Orange lines represent the evolution of an air mass that has experienced Rayleigh distillation for RH = 80 % and SST = 18 °C (thin line) and SST = 25 °C (thick line) respectively. These temperatures cover the annual mean sea surface temperatures around the Canaries. The thin black line represents the mixing between a moist air mass (initial conditions: H₂O = 18 000 ppmv, δ D = -84 ‰) and a dry air mass (initial conditions: H₂O = 400 ppmv, δ D = -600 ‰). The thick black line represents another mixing process (initial conditions for moist end member: H₂O = 16 000 ppmv, δ D = -93 ‰; initial conditions for dry end member: H₂O = 400 ppmv, δ D = -600 ‰).

dust measurements, and 70 % of TDE measurements. The H₂O- δ D pairs collected under dust-laden conditions were confined to the upper part of the distribution (red dots in Figs. 5 and 6). During these events, relatively enriched and moist H₂O- δ D pairs were measured. Mean values for IZO were -133 ± 35 ‰ for IZO and 7000 ± 3000 ppmv; and for TDE -152 ± 44 ‰ and 5000 ± 2000 ppmv respectively. The H₂O- δ D distribution under dust-laden events is limited by theoretical lines that simulate the mixing between BL and FT air. The dashed black line drawn in Figs. 5 and 6 represents the mixing between the following air masses: air mass (1) H₂O = 16 000 ppmv, δ D = -93 ‰ and air mass (2) H₂O = 400 ppmv, δ D = -600 ‰. This mixing line was determined as best fit of the border of the data of dust-laden air.

Episodes of moderate dust content ($2 < \text{dust} < 25 \mu\text{g m}^{-3}$, $0.02 < \text{AOD} < 0.1$) are related to air masses that have travelled westward from the African continent towards the Atlantic Ocean and then return eastward laden with the remaining dust, where they are measured at IZO. These events

are the mixing product of clean North Atlantic and Saharan dust-laden air masses. As a consequence, they do not make a unique fingerprint on the H₂O- δ D distribution and are not shown here.

Dust-laden Saharan air masses contribute to moisten the dry subtropical North Atlantic FT. The information of the H₂O- δ D pairs measured under these conditions indicate typical dehydration/mixing process also observed over the ocean. The transport of dust starts over the Sahara desert, where dust storms are driven by local thermal low pressure systems at the surface. In summer, the northward shift of the north-eastern trade winds and the intertropical convergence zone (ITCZ) in combination with a convective boundary layer prompts the strong injection of dust at high altitudes (Guirado et al., 2014; Rodríguez et al., 2015). The dust is then exported westwards at subtropical latitudes (20–30° N) within the Saharan Air Layer (SAL), a stratum of warm dust-laden air, normally located between an altitude of 1 to 5 km with a maximum dust load at an altitude between 2 and 3 km (e.g. Prospero et al., 2002; Rodríguez et al., 2011; Andrey

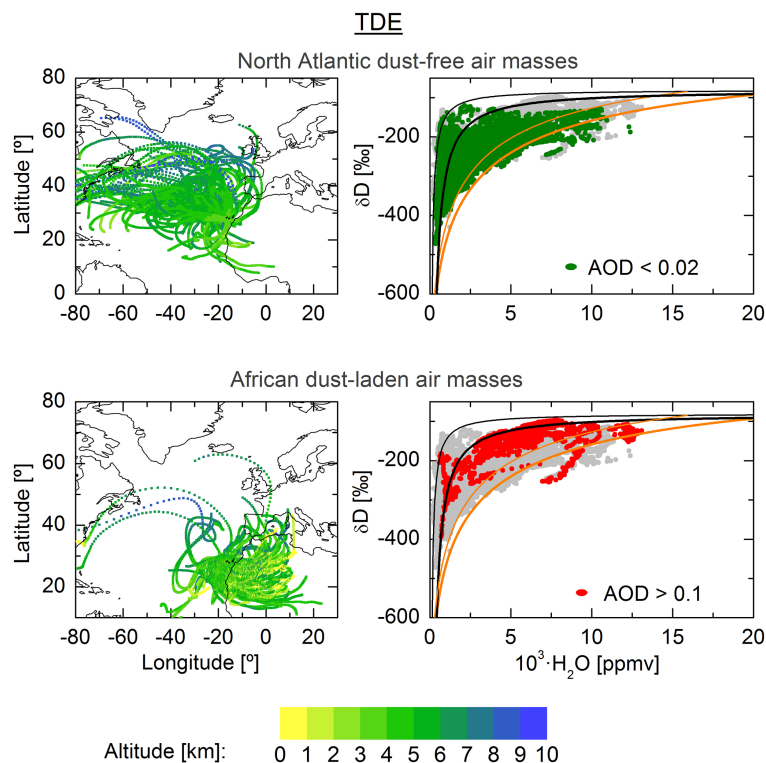


Figure 6. Same as Fig. 5 for the data collected at TDE station.

et al., 2013; Rodríguez et al., 2015). Previous work indicates that the moisture content of the SAL during summer has its origin in evaporation of the warmer Mediterranean Sea, which is then driven by the trade winds over north Africa, mixed with dust in the Sahara desert and then transported into the SAL to the subtropical North Atlantic FT (Millán et al., 1997, 2004; Rodríguez et al., 2011). Risi et al. (2010) showed column vapour δ D summer mean from satellite observations and atmospheric models varying between -100 and -160 ‰ for the region covering the Mediterranean Sea and the Sahara desert (period 2003–2005). These mean values are in agreement with our data set.

3.3 Classification of North Atlantic air masses as a function of the last condensation temperature

In this section, we focus on the moisture transport pathways over the North Atlantic. For this purpose, we only work with air masses corresponding to clean conditions (not linked to SAL) and we use the theory of the last condensation (LC) point. According to this theory, the mixing ratio is determined by the specific humidity at the point of LC, in which case it is not affected by subsequent mixing (Galewsky et al., 2005, and references therein).

We use GDAS1 data and HYSPLIT back trajectories to derive information about the LC point and mixing after LC and then relate this information to our H₂O- δ D observations. The

LC point is identified at the area where RH exceeds 80 % during a 3 h time interval (James et al., 2004; Sodemann et al., 2008). We use the corresponding 3 h averages of temperature and specific humidity at this LC point (in the following referred to as T_{LC} and $H_{2O_{LC}}$) for classifying the air masses.

We create three main data groups: $T_{LC} < 250$ K, $250 \text{ K} < T_{LC} < 270$ K, and $T_{LC} > 270$ K. The temperatures $T_{LC} = 250$ K and $T_{LC} = 270$ K correspond to humidities of approximately 1700 and 8000 ppmv respectively. The exact values of the temperatures that define the three temperature groups are more or less arbitrary. The absolute value is not important here. What is important is that we distinguish air masses according to their temperatures at the last condensation point. We group all air masses for low T_{LC} (last condensation at low temperatures, i.e. dry at the last condensation point) and for high T_{LC} (i.e. last condensation at high temperatures and accordingly humid air masses). Furthermore, we create a group that lies in between.

The top panels of Fig. 7 (left for IZO and right for TDE) show that T_{LC} is a good proxy for the locations of the LC point, since the data groups automatically with respect to the location and humidity of the last condensation point. The coldest saturation temperatures (220–250 K, blue) typically correspond to air transported from the upper extra-tropical troposphere ($> 40^\circ$ N, < 450 hPa). These air masses represent 32 and 43 % of the air masses reaching IZO and TDE station respectively. Air masses experiencing LC at warmer

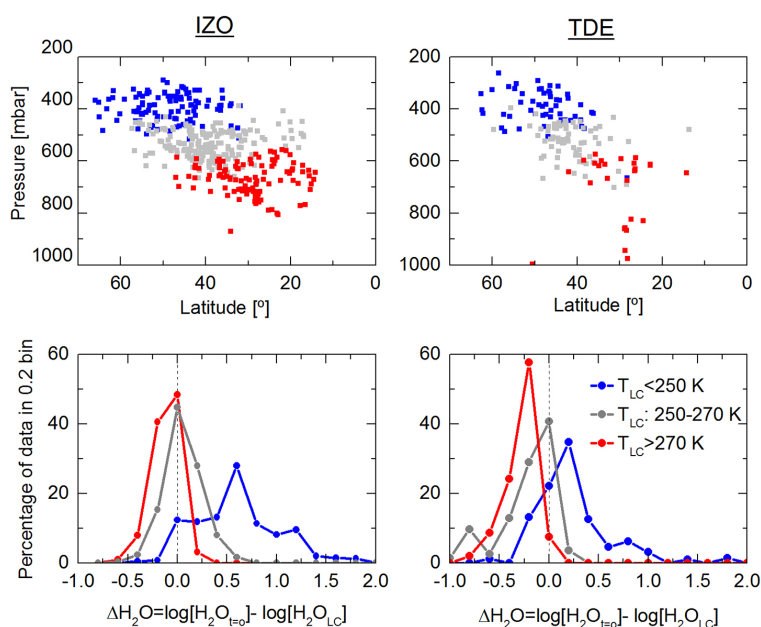


Figure 7. Trajectory-based analysis of the last condensation (LC) point for non-SAL conditions. Upper panels: location (pressure-latitude) of LC point. Bottom panels: histograms for $\Delta\text{H}_2\text{O} = \log[\text{H}_2\text{O}_{t=0}] - \log[\text{H}_2\text{O}_{\text{LC}}]$. The different colours correspond to different T_{LC} groups: $T_{\text{LC}} < 250$ K (blue line), $250 \text{ K} < T_{\text{LC}} < 270$ K (grey line) and $T_{\text{LC}} > 270$ K (red line).

temperatures (250–270 K) usually originate between 20 and 50° N at 400–600 hPa (grey, Fig. 7). They represent 48 and 42 % of the air masses reaching IZO and TDE respectively. The warmest LC temperatures (270–290 K) usually originate between 0 and 40° N and pressure levels above 600 hPa (red, Fig. 7). They represent 20 and 14 % of the air masses reaching IZO and TDE respectively.

We use the logarithmic difference between the humidity given by GDAS1/HYSPLIT at the station ($\text{H}_2\text{O}_{t=0}$) and the humidity at the LC point ($\text{H}_2\text{O}_{\text{LC}}$), in order to analyse if the air mass experienced variations on the moist content during the transport from the LC point to the stations ($\log[\text{H}_2\text{O}_{t=0}] - \log[\text{H}_2\text{O}_{\text{LC}}]$, hereafter $\Delta\text{H}_2\text{O}$). We postulate that the air masses with $\Delta\text{H}_2\text{O}$ within the ± 0.1 bin do conserve the properties of the LC point during their transport to IZO and TDE. Negative $\Delta\text{H}_2\text{O}$ indicates that the air masses mix with drier air masses during transport to the stations (we exclude situations of rainout by requiring that RH never reaches 80 % before the LC point). Positive $\Delta\text{H}_2\text{O}$ indicates that the air masses get moister. The bottom panels of Fig. 7 show the normalized distribution of $\Delta\text{H}_2\text{O}$ for the three T_{LC} groups (blue, black, and red coloured lines respectively). Left panel for IZO and right panel for TDE.

At IZO the humidity concentrations since the LC point are best conserved for $T_{\text{LC}} > 250$ K (red and grey lines). At TDE we observe a relatively clear moistening for $T_{\text{LC}} < 270$ K (grey and blue lines) and in general a drying for air masses with $T_{\text{LC}} > 270$ K (red line). The total contribution of air masses with $\Delta\text{H}_2\text{O} < -0.1$ (i.e. drying since LC) is 19 % at IZO and 43 % at TDE, revealing that drying by mixing with

dry air is more frequently observed at IZO. For $T_{\text{LC}} > 270$ K, i.e. for air that has been rather humid at the LC point, the drying by mixing with subsiding dry air is very clearly observed at TDE (red line, bottom right panel of Fig. 7). The total contribution of air masses with $\Delta\text{H}_2\text{O} > +0.1$ (i.e. moistening since LC) is 46 % at IZO and 29 % at TDE. This moistening is most pronounced for air with the LC point in the upper troposphere of the extra-tropics ($T_{\text{LC}} < 250$ K) and it becomes particularly evident at IZO (blue line, bottom left panel of Fig. 7). This moistening process is more important at IZO than at TDE, due to IZO's location at a lower altitude, which is directly affected by turbulent mixing from the marine boundary layer.

Figure 8 shows the H₂O-δD distribution as measured at IZO for the different T_{LC} groups. The H₂O-δD data pairs correspond to 10 min averages measured within ± 3 h of the air mass arrival time of the trajectory. For each T_{LC} group, the H₂O-δD data points have been colour-coded as a function of $\Delta\text{H}_2\text{O}$. Green highlights those data associated with $\Delta\text{H}_2\text{O}$ within ± 0.1 , thus conserving water vapour concentrations since LC. Dark grey marks data with $\Delta\text{H}_2\text{O}$ out of the ± 0.1 range. Figure 9 shows the same for the station TDE.

For the cold LC temperatures ($T_{\text{LC}} < 250$ K) and at TDE we typically observe dry air ($\text{H}_2\text{O} < 3000$ ppmv, see left panels in Fig. 9). For IZO we also observe dry air if there has been no mixing since LC ($\Delta\text{H}_2\text{O} \pm 0.1$, green dots, upper left panel in Fig. 8). However, this is only the case for about 14 % of all the air masses that have their LC at these low temperatures. This extratropical subsiding dry air has already been reported in other subtropical free troposphere stations in the

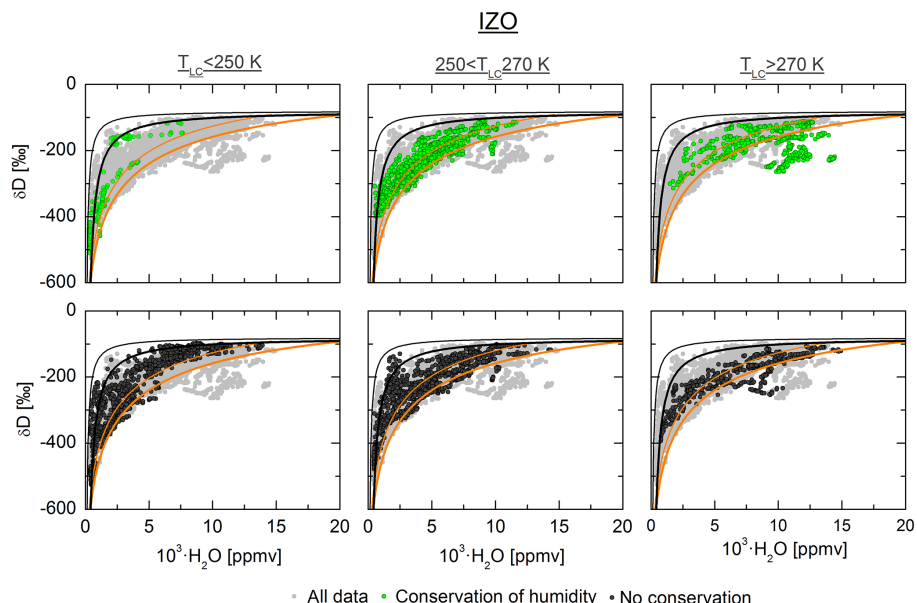


Figure 8. H₂O- δ D distribution (10 min data within ± 3 h of the arrival time of the air mass) measured at IZO station and analysed with regard to the LC point. The data set has been grouped in three groups corresponding to different condensation temperatures: $T_{LC} < 250$ K, $250 \text{ K} < T_{LC} < 270$ K and $T_{LC} > 270$ K. The H₂O- δ D pairs measured for reduced mixing since LC ($\Delta H_2O \pm 0.1$) are presented in green. Pairs measured for increased mixing since LC (ΔH_2O outside ± 0.1) are presented in dark grey. Rayleigh and mixing curves are plotted as in Figs. 5 and 6.

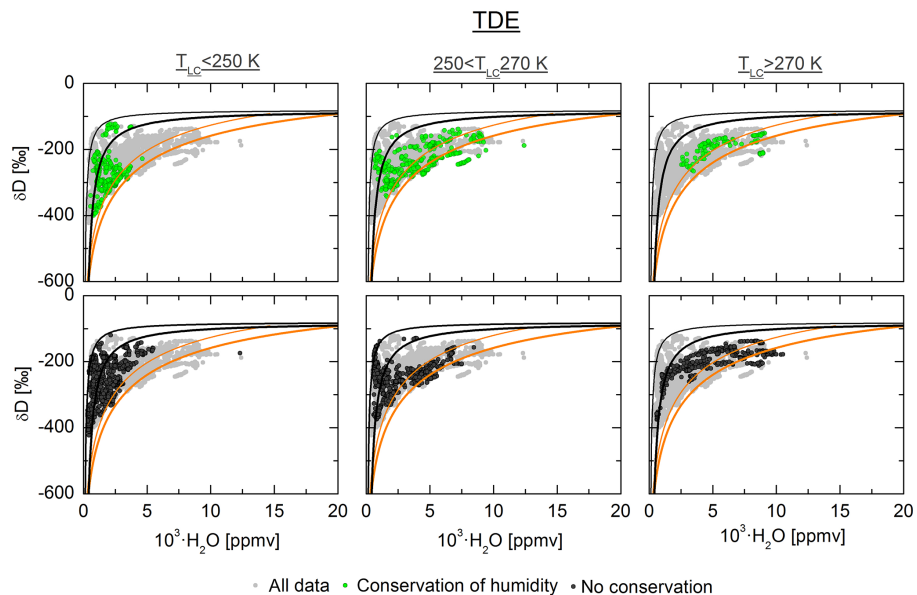


Figure 9. Same as Fig. 8 for the data collected at TDE station.

Pacific such as Chajnantor plateau (in Chile, Samuels-Crow et al., 2014) and Mauna Loa station (in Hawaii, e.g. Noone et al., 2011; Bailey et al., 2015). Generally at IZO humidity is not conserved since LC if T_{LC} is low. In most cases these air masses are mixed with humid air during their transport. This mixing can then be observed in the measured H₂O- δ D pairs. If there is a lot of mixing ($H_2O > 8000$ ppmv) the vapour is

clearly enriched in HDO, which is consistent with moistening by mixing with humid air (dark grey dots in the bottom left panel of Fig. 8). At the subtropical Pacific FT Mauna Loa station, Bailey et al. (2015) also showed that higher-latitude air masses are more humid than expected and attributed this to local mixing processes.

For the warmest LC temperature group ($T_{LC} > 270$ K, right panels in Fig. 8) we occasionally observe H₂O- δ D pairs below the exemplary Rayleigh distribution, which can be explained by evaporation from a rather warm ocean or by re-evaporation of falling rain droplets. Under these conditions the subtropical North Atlantic free troposphere is particularly humid. These tropical air masses moving north-east towards the Canaries, moistening the atmosphere, are also observed in the subtropical Pacific (in Mauna Loa station, Bailey et al., 2015). In some occasions, mixing with air from higher atmospheric levels can also dry these air masses. The distribution of H₂O- δ D pairs describing this mixing lie above the exemplary Rayleigh line (dark grey dots in bottom right panels of Figs. 8 and 9).

For air masses linked to intermediate T_{LC} (above 250 and below 270 K; central column in Figs. 8 and 9) we observe a mix of the different processes discussed above.

It is important to keep in mind that the meteorological parameters upwind of the stations as deduced by HYSPLIT/GDAS1 are the result of a dispersion model and analysis fields, each with an uncertainty. It is likely that our analyses are affected by these uncertainties. See more details in Appendix C. Nevertheless, we are able to demonstrate a clear relation between the HYSPLIT/GDAS1 data and the measured H₂O- δ D pairs which a posteriori justifies our approach. Our simplified analysis suggests that the distribution of the moisture in the subtropical North Atlantic FT is controlled by the temperature at last condensation and subsequent mixing of air masses. Thus, these results are in agreement with the idealized advection-condensation model proposed by Galewsky and Hurley (2010).

4 Summary and conclusions

We report continuous measurements of water vapour isotopologues made at two mountain observatories (IZO at 2370 m and TDE at 3550 m a.s.l.) on the island of Tenerife. We assume that the measurements made in the second half of the night are only very weakly affected by the local circulation on the island and represent the FT well. This assumption is consistent with previous studies of trace gases made on the island's mountain and it is also consistent with the wide distribution of the H₂O- δ D pairs corresponding to the night-time observations. Thus, our measurements generate a unique continuous water vapour isotopologue data record for the lower/middle FT and can be used for studying free-tropospheric water pathways. In this paper we perform such a study and therefore combine the isotopologue data with back trajectory calculations and dust measurements.

The distribution of water vapour isotopologues collected during dust-free North Atlantic conditions show wide variability. This variability has been analysed in the context of the last condensation point. The results show that the lowest δ D values registered at IZO are found in relation to air

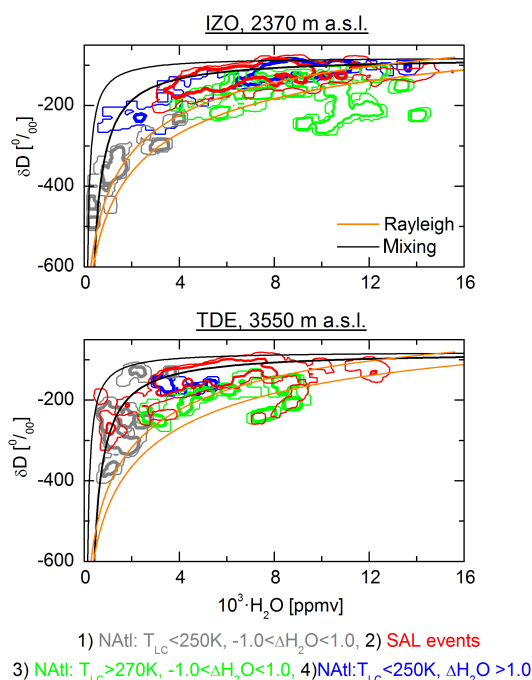


Figure 10. H₂O- δ D distributions as obtained for the four different moisture pathways that determine the free troposphere moisture budget in the surroundings of Tenerife (Left panel for IZO and right panel for TDE). Contour lines indicate the areas of highest data point density. The thin dashed and thick solid lines mark the areas that include 95 and 66 % of all data respectively. The different colour of the contour lines mark the different pathways (1–4) as given in the legend. Rayleigh and mixing curves are plotted as in Figs. 5, 6, 8, and 9.

masses that have experienced condensation at lower temperatures, and at higher latitudes and altitudes over the North Atlantic Ocean ($T_{LC} < 250$ K, $> 40^\circ$ N, < 400 hPa). The condensation at low temperatures is responsible for the dryness of the subtropical North Atlantic FT. These air masses seem to frequently experience mixing with more humid air masses during transport to the subtropical region. Moistening during subsidence was detected by analysing GDAS1/HYSPLIT data and identified in the measured H₂O- δ D distribution. Humid air masses are also detected when the last condensation takes place close to the surface at lower latitudes not far from the Canaries (> 270 K, > 600 hPa), whereby the observed H₂O- δ D distribution indicates rain re-evaporation or evaporation over a warm ocean as moisture source (increased depletion with respect to Rayleigh).

For dust episodes, rather humid and enriched vapour is detected at the stations, indicating a strong injection of boundary layer air into the FT. These dust-laden air masses, which are the product of a strong convection over the Sahara desert, reach the Canaries without having experienced significant condensation and are found as an influential contribution for moisture in this region. We show that the measurements of

water vapour isotopologues at regions located to the west of the African continent provide new insights into the influence of the African continent on the moisture budget of the subtropical Northern Atlantic FT.

In summary, our results indicate that four different moisture transport pathways have to be considered in order to understand the subtropical North Atlantic moisture budget. While the dominant dryness of the region is determined by the mean subsidence of dry air from high altitudes of the extra-tropics (pathway 1), there are three main processes that moisten the FT over the Atlantic: horizontal mixing over the Atlantic with air from the Saharan Air Layer (pathway 2), transport of air from low altitudes ($P > 600$ hPa) and latitudes (whereby humidity occasionally originates from rain-evaporation, pathway 3), and vertical mixing close to the Canaries (pathway 4).

Figure 10 gives an overview on the H₂O-δD distributions as observed when one of the four different pathways is clearly prevailing. It depicts the areas with the highest density of the observed H₂O-δD pairs. Pathway 2 dominates when there is high aerosol load (dust $> 25 \mu\text{g m}^{-3}$ or AOD > 0.1 , red contour lines). The other pathways dominate for low aerosol load (dust $< 2 \mu\text{g m}^{-3}$ or AOD < 0.02) and when T_{LC} and $\Delta\text{H}_2\text{O}$ are situated within specific ranges.

Pathway 1 prevails for $T_{LC} < 250$ K and $\Delta\text{H}_2\text{O}$ within ± 0.1 (grey contour lines). Pathway 3 prevails for $T_{LC} > 270$ K and $\Delta\text{H}_2\text{O}$ within ± 0.1 (green contour lines). Finally pathway 4 dominates for $T_{LC} < 250$ K and $\Delta\text{H}_2\text{O} > 1.0$ (blue contour lines). This pathway is mainly limited to altitudes below 3000 m a.s.l., and it is more frequently observed at IZO than at TDE. In the range of high humidity, pathways 2 and 4 are difficult to distinguish, because both pathways show the mixing product between dry and humid air masses. The use of aerosol measurements allows us to distinguish these two situations and also gives new insights into the properties of the air masses over the Sahara desert and their subsequent advection over the Atlantic Ocean.

The summary as shown in Fig. 10 reveals that the H₂O-δD pairs measured in the subtropical North Atlantic FT well reflect the dominating moisture transport pathways to this atmospheric region. A continued long-term monitoring of water vapour isotopologue ratios would offer a unique possibility for investigating the importance of the different mechanisms responsible for the expected moistening of the subtropical North Atlantic FT in response to climate change.

Appendix A: Calibration procedure of Picarro instruments

A1 Mixing ratio calibration

Measurements of absolute humidity obtained from the meteorological sensors have been used for correcting Picarro humidity measurements. The meteorological stations are located close to respective Picarro inlets. The temperature and relative humidity of these stations have been used for calculating the water vapour pressure ($e = e_{\text{sat}} \cdot \text{RH}/100$). The saturation vapour pressure is calculated from the Magnus–Tetens formula ($e_{\text{sat}} = 6.1094 \cdot \exp(17.625 \cdot T)/(243.04 + T)$, WMO, 2008).

Figure A1 shows 1 h resolution of simultaneous measurements of humidity from the meteorological station and the Picarro at IZO and TDE stations respectively. The slope (S), intercept (i), and coefficient of determination (r^2) of the linear fit at each station are shown. The linear fit obtained at each station is applied for correcting the Picarro humidity measurements.

A2 Isotopic calibrations with the SDM system

Calibration measurements are carried out every 8–12 h by sequentially measuring the two working standards at three different water vapour mixing ratios of around 6000, 12 000, and 18 000 ppmv using a Picarro SDM. Therein, a micro-litre volume of liquid working standard is injected into a heated oven where it evaporates completely without fractionation. It is subsequently diluted into a flow of dry synthetic air. The amount of liquid working standard can be adjusted in a certain range and, together with the flow rate of synthetic air, determine the humidity of the calibration gas mixture produced. This calibration gas mixture is then measured by the Picarro spectrometer for 20 min at each humidity level. A 6 min time interval is discarded between ambient and calibration measurements, as well as between different humidity levels and working standards. This allows for appropriate isotope and humidity exchange in the measurement cell of the Picarro spectrometer. The calibration procedure thus takes slightly over 2 h.

The calibration frequency, as well as the calibration humidity levels, have been modified slightly during the course of our measurements depending on demands during certain campaign periods. At TDE, the airflow is controlled by an electronic mass flow controller, while at IZO the flow is controlled by a rotameter. The reduced precision of this second device is translated in a larger variability of the calibration humidity at IZO in comparison to TDE (Fig. A2).

In order to apply the calibration gas measurements to our ambient measurements, we first filter out calibration measurements where any of the syringes of the SDM was clogged. We then analyse the humidity dependence of the measured raw isotope ratios during calibration, using the

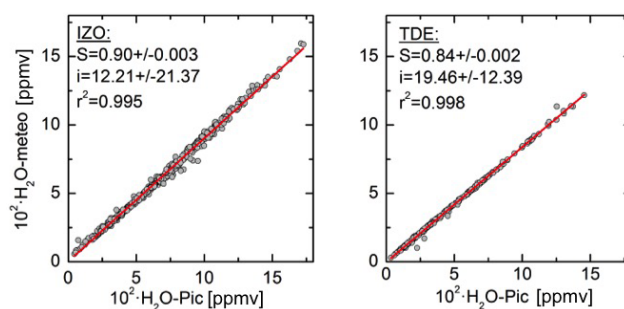


Figure A1. Grey dots show the 1 h humidity data pairs of the Picarro and the meteorological at IZO and TDE. Red lines indicate the linear fit of the distribution. S = slope, i = intercept, r^2 = coefficient of determination.

three recorded humidity levels. If a humidity dependence significantly larger than the precision of the calibration measurements was found, we would have to apply a correction function. This was not the case for our calibration measurements. Figure A3 shows an example measurement of humidity dependence of δD at IZO and TDE stations respectively. An uncalibrated working standard was used in a bubbler to saturate synthetic air with water vapour. This air was then diluted into a variable flow of synthetic air to produce a gas mixture of variable humidity. The data are averaged for 1 min, and the error bars denote the 1σ -standard deviation of the δD measurements. For low humidity measurements, where the instrument is most susceptible to a humidity dependence of δD , the dependence remains within the scatter of the data (1σ standard deviation). Please also be aware that we use a Picarro L-2120i model. The Picarro models L-21xxi have significantly less dependency on humidity concentrations than the Picarro models L-11xxi (e.g. Aemisegger et al., 2012).

The stability of the humidity dependence for SDM calibrations along the whole study period is shown in the left column of Fig. A2. We analyse the differences obtained from the regular calibrations made below and above 15 000 ppmv. No significant differences are observed along the humidity range covered with the SDM, being the 3σ below 0.8 ‰ at IZO (1.8 ‰ at TDE) (instrumental precision < 0.5 ‰).

Subsequently we determine a linear regression function of the two working standards S1 and S2 measured during calibration (Fig. A4). This function is of the form $\delta\text{D}_{\text{VSMOW}} = a + b \times \delta\text{D}_{\text{measured}}$, and it takes the uncertainty of the isotopic composition of the working standards as well as the precision of the calibration measurements into account. We determine a calibration function for every calibration measurement described above (1 to 2 per day). We apply this function to the ambient measurements in order to transfer these measurements onto the VSMOW2/SLAP2 scale. The uncertainty in this linearity is about ± 2 ‰ (determined with standards between +15 and -428 ‰, (see Fig. 2 of Aemisegger et al., 2012). Since our working standards cover 100 ‰,

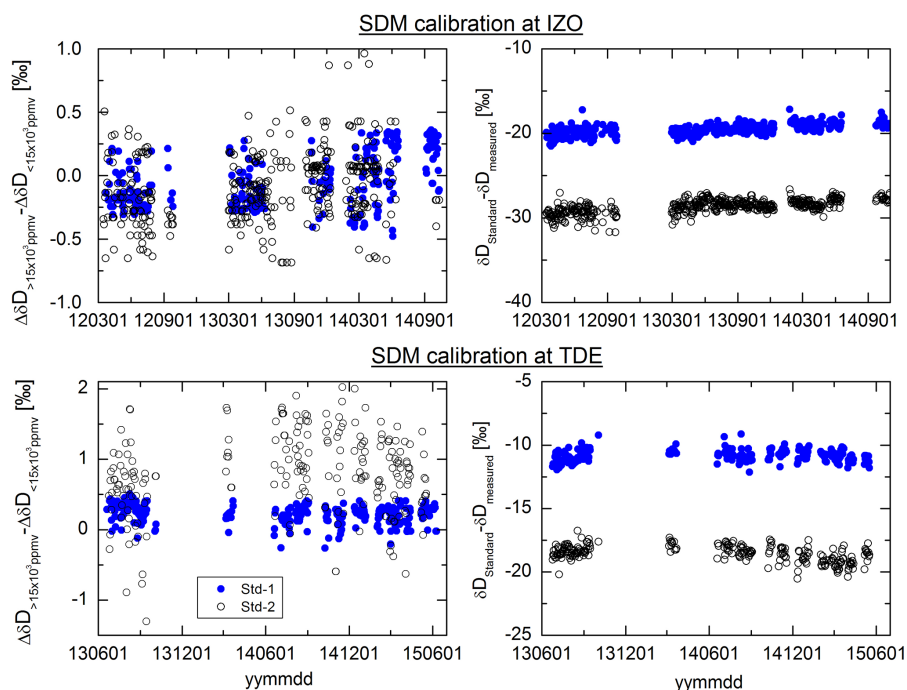


Figure A2. Difference between the measured δ D and that from the two liquid standards used for calibrating the instruments at IZO (first row) and TDE stations (second row). The left column depicts the dependence of this difference to the humidity during calibration. The right column shows the evolution of the difference with the time for all humidity levels.

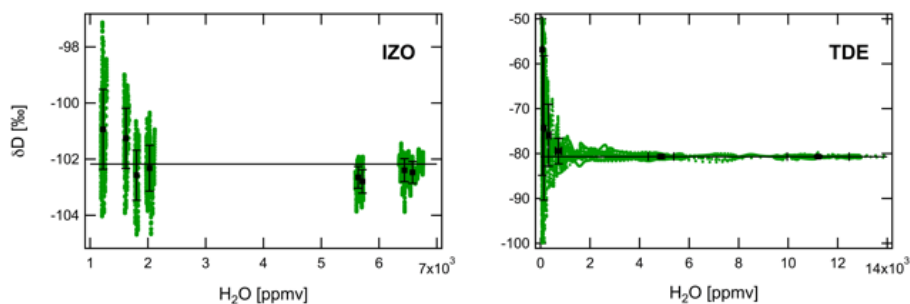


Figure A3. Measured humidity dependence of δ D determined by measuring water vapour produced in a bubbler dilution system at IZO (left) and TDE (right) stations respectively. Data shown are 1 min averages. The error bars indicate the 1σ standard deviation of the δ D measurements, within which the average δ D of each humidity bin (black symbols) are identical to the average of all data.

the uncertainty in slope (a) of the aforementioned calibration function is 2 ‰/100 ‰.

Each day, the data are calibrated with the resulting combination of the calibration at three different humidity points (no humidity dependence was found) and a linear fit between the responses of the two standards. The right column of this figure shows the time series of the SDM calibrations carried out at IZO and TDE stations (gaps are due to instrumentation repairs). No temporal drifts are observed in the different time series, indicating that both Picarro instruments are very stable and consistent over time.

For the total uncertainty estimation we consider the instrumental precision as well as uncertainty components:

- uncertainty of the standards (0.7 ‰ for both dry and humid air),
- humidity dependence (from 0.3 ‰ for 10 000 ppmv, up to 8.0 ‰ at 200 ppmv),
- extrapolation of VSMOW2-SLAP2 scale outside the range of calibration (for humid air: < 2.0 ‰; up to 5 ‰ for strong depleted air),
- calibration (1 ‰ for the whole humidity range).

The absolute uncertainties in δ D are then < 14.7 ‰ for strong depleted air at 500 ppmv and < 4 ‰ at 4500 ppmv.

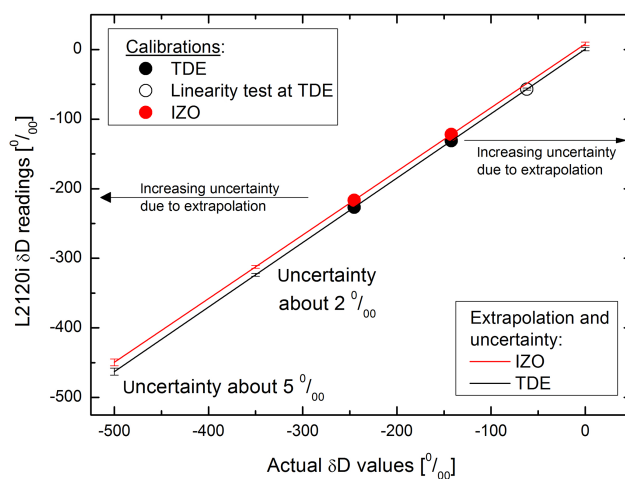


Figure A4. Schematic graph showing the use of two isotope working standards S1 and S2 with known δD_{VSMOW} . When the two standards are measured by an instrument one obtains $\delta D_{\text{measured}}$. A linear regression of the form $y = a + bx$ can be used to transfer $\delta D_{\text{measured}}$ onto the VSMOW scale. Note that uncertainties in x and y are considered.

Appendix B: Diurnal signals as seen in H₂O-δD distribution density plots

Figure 4 shows all the observed 10 min averaged H₂O-δD data pairs, which is a large amount of data (about 75 000 and 40 000 data points at IZO and TDE respectively). From Fig. 4 it becomes clear that the IZO daytime observations cover only a limited area in the H₂O-δD distribution space. There is no single IZO daytime observation with δD below -345 ‰ (and almost no daytime observations with δD below -220 ‰ for H₂O above 10 000 ppmv). For TDE the situation is not clear from Fig. 4.

In order to give a statistical insight into the differences between the H₂O-δD distributions during day and night, we additionally calculate the density of the H₂O-δD distributions for the daytime and night-time data pairs. The respective distribution plots are shown in Fig. B1 and clearly confirm that for IZO the daytime and night-time H₂O-δD distributions are significantly different. For TDE the day-night differences are less pronounced, but they become visible in the density plot (right panel of Fig. B1). For instance, at TDE the probability for δD being below -300 ‰ is significantly higher during night than during day (compare the areas marked by the thick black and orange lines).

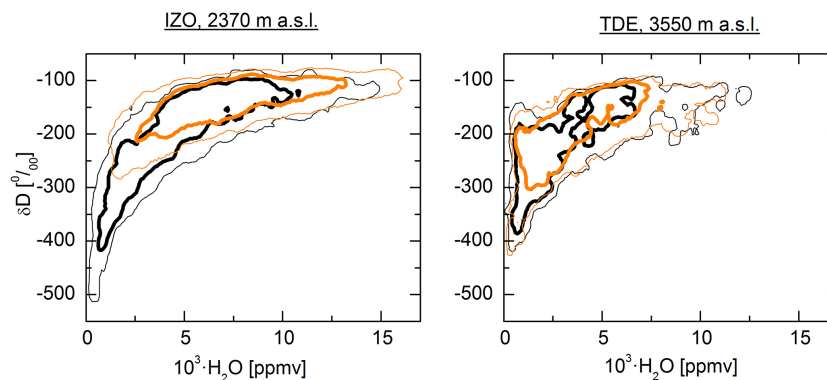


Figure B1. H₂O-δD distributions as obtained for the “night-time observation” (10 min averages made between midnight and 1 h after sunrise, black contour lines) and the “daytime observations” (10 min averages made between 3 and 10 h after sunrise, orange contour lines). The thin and thick lines mark areas that include 95 and 66 % of all the data. The plot shows the density distributions of the data points from Fig. 4.

Appendix C: Discussion of the representativeness of the used T_{LC} and ΔH_2O parameters

There are two different reasons for a not perfect representativeness: First, there is an uncertainty in the trajectories, which is the larger the longer the trajectory. Second, the model does not well resolve the fine structured topography of Tenerife, which might affect the flow of air masses and already the height attribution of the trajectories might be incorrect.

In our case, the trajectories are released at the height above sea level of the stations. We tested the uncertainty we could have in the representativeness of our backward trajectories by looking also in the backward trajectories released 500 m above and 500 m below. The data set describes those days in which last condensation has been observed along the pathways at the three altitudes (only during the night-time period, 00:00 and 06:00 UTC), and we calculate for all trajectories the parameters T_{LC} and $\Delta H_2O = \log(H_2O_{t=0}) - \log(H_2O_{LC})$.

The test is made for the TDE station and we correlate the parameters as obtained at 3500 m (altitude of the site), with the parameters as obtained at 4000 m (blue stars in Figs. C1 and C2) and 3000 m (red stars). The green line represents the diagonal (3500 m). The uncertainty test was carried out with 3 years of back trajectories (2012–2014). The Pearson's coefficients obtained for T_{LC} and ΔH_2O (for each of the three T_{LC} categories) are shown in the figures.

The scatter in the plots documents the uncertainty in the representativeness of the T_{LC} and ΔH_2O as used in our study. However, we think that this scatter is a conservative uncertainty estimation. The reason is that we work with night-time data (midnight – one hour after sunrise). During that time the atmosphere above the island is rather stable and local effects (not resolved by the model) should by far be less important than during the daytime. That is we think that the air mass recorded during night-time the stations IZO and TDE corresponds to air travelling over the ocean around the island at very similar altitudes and the scatter for altitude differences of as large as ± 500 m likely overestimates the actual uncertainty.

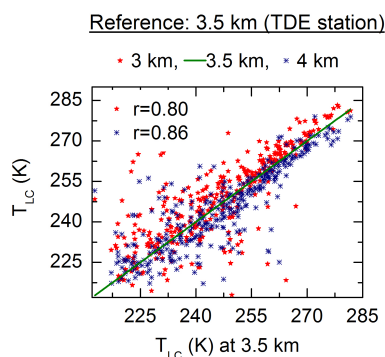


Figure C1. A 3-year (2012–2014) analysis of the uncertainty in the vertical resolution of the model using TDE as reference station. The correlation between T_{LC} at 3500 m with 3000 and 4000 m respectively, is shown.

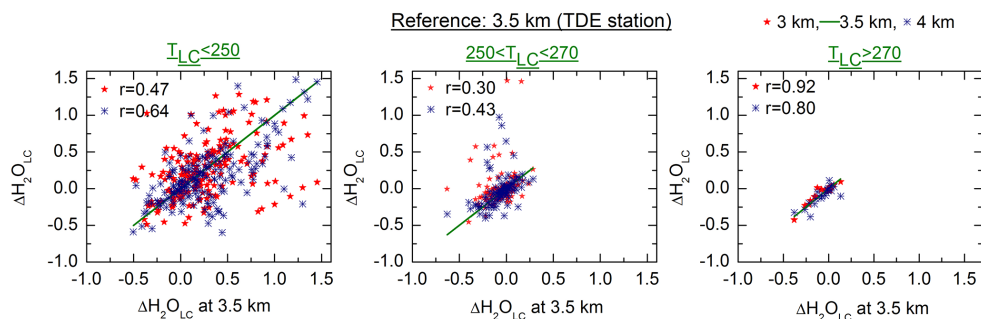


Figure C2. A 3-year (2012–2014) analysis of the uncertainty in the vertical resolution of the model using TDE as reference station. The correlation between $\Delta H_2O = \log[H_2O'_{t=0}] - \log[H_2O_{LC}]$ at 3500 m with 3000 and 4000 m respectively, is shown.

Acknowledgements. This study has been conducted in the framework of the project MUSICA (MULTi-platform remote Sensing of Isotopologues for investigating the Cycle of Atmospheric water), funded by the European Research Council under the European Community's Seventh Framework Programme (FP7/2007-2013/ERC Grant agreement number 256961). We thank Dan Smale (NIWA, New Zealand) and the staff of Arrival Heights/Scott Base for providing the Antarctic ice water probes we used for preparing our isotopologue standards. The isotopologue composition of the probes was kindly determined by LSCE-CEA, France. Aerosol measurements are part of the project POLLINDUST (CGL2011-26259), funded by the Minister of Economy and Competitiveness of Spain. The AERONET sun photometer at Izana (PI: Emilio Cuevas) has been calibrated within AERONET EUROPE TNA supported by the European Community Research Infrastructure Action under the FP7 Capacities programme for Integrating Activities, ACTRIS grant agreement number 262254. Eliezer Sepúlveda is supported by the NOVIA project (Ministerio de Economía y Competitividad of Spain, CGL2012-37505). We thank the editor and the three anonymous referees for their very constructive input and their help in improving the presentation of our results.

Edited by: H. Wernli

References

- Aemisegger, F., Sturm, P., Graf, P., Sodemann, H., Pfahl, S., Knohl, A., and Wernli, H.: Measuring variations of $\delta^{18}\text{O}$ and $\delta^2\text{H}$ in atmospheric water vapour using two commercial laser-based spectrometers: an instrument characterisation study, *Atmos. Meas. Tech.*, 5, 1491–1511, doi:10.5194/amt-5-1491-2012, 2012.
- Andrey, J., Cuevas, E., Parrondo, M., Alonso-Pérez, S., Rondas, A., and Gil-Ojeda, M.: Quantification of ozone reductions within the Saharan air Layer through a 13-year climatologic analysis of ozone profiles, *Atmos. Environ.*, 84, 28–34, doi:10.1016/j.atmosenv.2013.11.030, 2013.
- Basart, S., Pérez, C., Cuevas, E., Baldasano, J. M., and Gobbi, G. P.: Aerosol characterization in Northern Africa, Northeastern Atlantic, Mediterranean Basin and Middle East from direct-sun AERONET observations, *Atmos. Chem. Phys.*, 9, 8265–8282, doi:10.5194/acp-9-8265-2009, 2009.
- Bailey, A., Toohey, D., and Noone, D.: Characterizing moisture exchange between the Hawaiian convective boundary layer and free troposphere using stable isotopes in water, *J. Geophys. Res.*, 118, 8208–8221, doi:10.1002/jgrd.50639, 2013.
- Bailey, A., Noone, D., Berkelhammer, M., Steen-Larsen, H. C., and Sato, P.: The stability and calibration of water vapor isotope ratio measurements during long-term deployments, *Atmos. Meas. Tech.*, 8, 4521–4538, doi:10.5194/amt-8-4521-2015, 2015.
- Benetti, M., Reverdin, G., Pierre, C., Merlivat, L., Risi, C., Steen-Larsen, H. C., and Vimeux, F.: Deuterium excess in marine water vapor: Dependency on relative humidity and surface wind speed during evaporation, *J. Geophys. Res.-Atmos.*, 119, 584–593, doi:10.1002/2013JD020535, 2014.
- Brown, D., Worden, J., and Noone, D.: Characteristics of tropical and subtropical atmospheric moistening derived from Lagrangian mass balance constrained by measurements of HDO and H₂O, *J. Geophys. Res.*, 118, 54–72, doi:10.1029/2012JD018507, 2013.
- Chiapello, I., Prospero, J., Herman, J., and Hsu, N.: Detection of mineral dust over the North Atlantic Ocean and Africa with the Nimbus 7 TOMS, *J. Geophys. Res.*, 104, 9277–9291, doi:10.1029/1998JD200083, 1999.
- Coplen, T. B.: Guidelines and recommended terms for expression of stable-isotope-ratio and gas-ratio measurement results, *Rapid Commun. Mass Sp.*, 25, 2538–2560, doi:10.1002/rcm.5129, 2011.
- Couhert, A., Schneider, T., Li, J., Waliser, D. E., and Tompkins, A. M.: The maintenance of the relative humidity of the subtropical free troposphere, *J. Climate*, 23, 390–403, doi:10.1175/2009JCLI2952.1, 2010.
- Craig, H.: Standard for Reporting concentrations of Deuterium and Oxygen-18 in natural waters, *Science*, 13, 1833–1834, doi:10.1126/science.133.3467.1833, 1961.
- Cuevas, E., González, Y., Rodríguez, S., Guerra, J. C., Gómez-Peláez, A. J., Alonso-Pérez, S., Bustos, J., and Milford, C.: Assessment of atmospheric processes driving ozone variations in the subtropical North Atlantic free troposphere, *Atmos. Chem. Phys.*, 13, 1973–1998, doi:10.5194/acp-13-1973-2013, 2013.
- Draxler, R. and Rolph, G.: HYSPLIT (HYbrid Single-Particle Lagrangian Integrated Trajectory) Model Access Via NOAA ARL READY, NOAA Air ReSOURCEs Laboratory, Silver Spring, MD Website, available at: <http://www.arl.noaa.gov/ready/hysplit4.html> (last access: June 2015), 2003.
- Dyroff, C., Sanati, S., Christner, E., Zahn, A., Balzer, M., Bouquet, H., McManus, J. B., González-Ramos, Y., and Schneider, M.: Airborne in situ vertical profiling of HDO/H₂¹⁶O in the subtropical troposphere during the MUSICA remote sensing validation campaign, *Atmos. Meas. Tech.*, 8, 2037–2049, doi:10.5194/amt-8-2037-2015, 2015.
- Galewsky, J. and Hurley, J. V.: An advection-condensation model for subtropical water vapour isotopic ratios, *J. Geophys. Res.*, 115, D16116, doi:10.1029/2009JD013651, 2010.
- Galewsky, J., Sobel, A., and Held, I.: Diagnosis of subtropical humidity dynamics using tracers of last saturation, *J. Atmos. Sci.*, 62, 3353–3367, 2005.
- García, O. E., Díaz, J. P., Expósito, F. J., Díaz, A. M., Dubovik, O., Derimian, Y., Dubuisson, P., and Roger, J.-C.: Shortwave radiative forcing and efficiency of key aerosol types using AERONET data, *Atmos. Chem. Phys.*, 12, 5129–5145, doi:10.5194/acp-12-5129-2012, 2012.
- Gómez-Peláez, A., Ramos, R., and Pérez-de la Puerta, J.: Methane and carbon dioxide continuous measurements at Izaña GAW station (Spain), in: GAW Report (No. 168) of the “13th WMO/IAEA Meeting of Experts on Carbon Dioxide Concentration and Related Tracers Measurement Techniques (Boulder, Colorado, USA, 19–22 September 2005)”, edited by: Miller, J. B., World Meteorological Organization (TD No. 1359), available at: <http://www.wmo.int/pages/prog/arep/gaw/gaw-reports.html> (last access: October 2014), 2006.
- Guirado, C., Cuevas, E., Cachorro, V. E., Toledano, C., Alonso-Pérez, S., Bustos, J. J., Basart, S., Romero, P. M., Camino, C., Mimouni, M., Zeudmi, L., Goloub, P., Baldasano, J. M., and de Frutos, A. M.: Aerosol characterization at the Saharan AERONET site Tamanrasset, *Atmos. Chem. Phys.*, 14, 11753–11773, doi:10.5194/acp-14-11753-2014, 2014.

- Holben, B. N., Eck, T. F., Slutsker, I., Tanré, D., Buis, J. P., Setzer, A., Vermote, E., Reagan, J. A., Kaufman, Y. J., Nakajima, T., Lavenu, F., Jankowiak, I., and Smirnov, A.: AERONET – a federated instrument network and data archive for aerosol characterization, *Remote Sens. Environ.*, 66, 1–16, 1998.
- IAEA (International Atomic Energy Agency): Reference Sheet for VSMOW2 and SLAP2 international measurement standards, available at: https://nucleus.iaea.org/rpst/documents/vsmow2_slap2.pdf (last access: January 2016), IAEA, 2009.
- James, P., Stohl, A., Spichtinger, N., Eckhardt, S., and Forster, C.: Climatological aspects of the extreme European rainfall of August 2002 and a trajectory method for estimating the associated evaporative source regions, *Nat. Hazards Earth Syst. Sci.*, 4, 733–746, doi:10.5194/nhess-4-733-2004, 2004.
- Johnson, D. G., Jucks, K. W., Trauba, W. A., and Chance, K. V.: Isotopic composition of stratospheric water vapor. Implications for transport, *J. Geophys. Res.*, 106, 12219–12226, 2001.
- Millán, M. M., Salvador, R., Mantilla, E., and Kallos, G.: Photooxidant dynamics in the Mediterranean basin in summer: results from European research projects, *J. Geophys. Res.*, 102, 8811–8823, 1997.
- Millán, M. M., Estrella, M., Sanz, M., Mantilla, E., Martín, M., Pastor, F., Salvador, R., Vallejo, R., Alonso, L., Gangotti, G., Ildardia, J., Navazo, M., Albizuri, A., Artiñano, B., Ciccio, P., Kallos, G., Carvalho, R., Andrés, D., Hoff, A., Werhan, J., Seufert, G., and Versino, B.: Climatic feedbacks and desertification: the mediterranean model, *J. Climate*, 18, 684–701, 2004.
- Noone, D., Galewsky, J., Sharp, Z., Worden, J., Barnes, J., Baer, D., Bailey, A., Brown, D., Christensen, L., Crosson, E., Dong, F., Hurley, J., Johnson, L., Strong, M., Toohey, D., Van Pelt, A., and Wright, J.: Properties of air mass mixing and humidity in the subtropics from measurements of the D/H isotope ratio of water vapor at the Mauna Loa Observatory, *J. Geophys. Res.*, 116, D22113, doi:10.1029/2011JD015773, 2011.
- Palmén, E. and Newton, C.: *Atmospheric Circulation Systems: Their Structure and Physical Interpretation*, Int. Geophys. Ser., 13, Academic Press, New York, 603 pp., 1969.
- Pierrehumbert, R.: Lateral mixing as a source of subtropical tropospheric water vapour, *Geophys. Res. Lett.*, 25, 151–154, 1998.
- Prospero, J., Ginoux, P., Torres, O., Nicholson, S. E., and Gill, T. E.: Environmental characterization of global sources of dust with the Nimbus 7 total ozone mapping spectrometer (TOMS) absorbing aerosol product, *Rev. Geophys.*, 40, 2.1–2.31, doi:10.1029/2000RG000095, 2002.
- Risi, C., Bony, S., Vimeux, F., Frankenberg C., Noone, D., and Worden, J.: Understanding the Sahelian water budget through the isotopic composition of water vapor and precipitation, *J. Geophys. Res.*, 115, D24110, doi:10.1029/2010JD014690, 2010.
- Risi, C., Noone, D., Worden, J., Frankenberg, C., Stiller, G., Kiefer, M., Funke, B., Walker, K., Bernath, P., Schneider, M., Bony, S., Lee, J., Brown, D., and Sturm, C.: Process-evaluation of tropospheric humidity simulated by general circulation models using water vapour isotopic observations: 2. Using isotopic diagnostics to understand the mid and upper tropospheric moist bias in the tropics and subtropics, *J. Geophys. Res.*, 117, D05304, doi:10.1029/2011JD016623, 2012.
- Rodríguez, S., González, Y., Cuevas, E., Ramos, R., Romero, P. M., Abreu-Afonso, J., and Redondas, A.: Atmospheric nanoparticle observations in the low free troposphere during upward orographic flows at Izaña Mountain Observatory, *Atmos. Chem. Phys.*, 9, 6319–6335, doi:10.5194/acp-9-6319-2009, 2009.
- Rodríguez, S., Alastuey, A., Alonso-Pérez, S., Querol, X., Cuevas, E., Abreu-Afonso, J., Viana, M., Pérez, N., Pandolfi, M., and de la Rosa, J.: Transport of desert dust mixed with North African industrial pollutants in the subtropical Saharan Air Layer, *Atmos. Chem. Phys.*, 11, 6663–6685, doi:10.5194/acp-11-6663-2011, 2011.
- Rodríguez, S., Alastuey, A., and Querol, X.: A review of methods for long term in situ characterization of aerosol dust, *Aeolian Res.*, 6, 55–74, doi:10.1016/j.aeolia.2012.07.004, 2012.
- Rodríguez, S., Cuevas, E., Prospero, J. M., Alastuey, A., Querol, X., López-Solano, J., García, M. I., and Alonso-Pérez, S.: Modulation of Saharan dust export by the North African dipole, *Atmos. Chem. Phys.*, 15, 7471–7486, doi:10.5194/acp-15-7471-2015, 2015.
- Rolph, G., Ngan, F., and Draxler, R.: Modeling the fallout from stabilized nuclear clouds using the HYSPLIT atmospheric dispersion model, *J. Environ. Radioactiv.*, 136, 41–55, 2014.
- Samuels-Crow, K. E., Galewsky, J., Sharp, Z. D., and Dennis, K. J.: Deuterium excess in subtropical free troposphere water vapor: continuous measurements from the Chajnantor Plateau, northern Chile, *Geophys. Res. Lett.*, 41, 8652–8659, doi:10.1002/2014GL062302, 2014.
- Schneider, M., González, Y., Dyroff, C., Christner, E., Wiegeler, A., Barthlott, S., García, O. E., Sepúlveda, E., Hase, F., Andrey, J., Blumenstock, T., Guirado, C., Ramos, R., and Rodríguez, S.: Empirical validation and proof of added value of MUSICA's tropospheric δ D remote sensing products, *Atmos. Meas. Tech.*, 8, 483–503, doi:10.5194/amt-8-483-2015, 2015.
- Sodemann, H., Schwierz, C., and Wernli, H.: Interannual variability of Greenland winter precipitation sources: lagrangian moisture diagnostic and North Atlantic Oscillation influence, *J. Geophys. Res.*, 113, D03107, doi:10.1029/2007JD008503, 2008.
- Steen-Larsen, H. C., Sveinbjörnsdóttir, A. E., Peters, A. J., Masson-Delmotte, V., Guishard, M. P., Hsiao, G., Jouzel, J., Noone, D., Warren, J. K., and White, J. W. C.: Climatic controls on water vapor deuterium excess in the marine boundary layer of the North Atlantic based on 500 days of in situ continuous measurements, *Atmos. Chem. Phys.*, 14, 7741–7756, doi:10.5194/acp-14-7741-2014, 2014.
- Steen-Larsen, H. C., Sveinbjörnsdóttir, A. E., Jonsson, Th., Ritter, F., Bonne, J.-L., Masson-Delmotte, V., Sodemann, H., Blunier, T., Dahl-Jensen, D., and Vinther, B. M.: Moisture sources and synoptic to seasonal variability of North Atlantic water vapor isotopic composition, *J. Geophys. Res.-Atmos.*, 120, 5757–5774, doi:10.1002/2015JD023234, 2015.
- Tremoy, G., Vimeux, F., Mayaki, S., Souley, I., Cattani, O., Risi, C., Favreau, G., and Oi, M.: A 1 year long ¹⁸O record of water vapor in Niamey (Niger) reveals insightful atmospheric processes at different timescales, *Geophys. Res. Lett.*, 39, L08805, doi:10.1029/2012GL051298, 2012.
- WMO: Guide to Meteorological Instruments and Methods of Observation, WMO Technical Publication No. 8, World Meteorological Organisation, Geneva, 2008.